URSI GASS 2020, Rome, Italy, 29 August - 5 September 2020

Magnetic Resonance Imaging using Optimized 2D Non-Uniform FFTs for spiral scanning

Amedeo Capozzoli, Claudio Curcio, Angelo Liseno
(1) Universitá di Napoli Federico II, Dipartimento di Ingegneria Elettrica e delle Tecnologie dell'Informazione,
via Claudio 21, I 80125 Napoli (Italy); e-mail: a.capozzoli@unina.it.

Abstract

In many recent applications of MRI, the acquisitions are performed by using spiral scans instead of Cartesian either to speedup the measurements or to make the hardware easier. In such a case, the complexity is dumped to processing which cannot profit anymore of the standard FFT. Non-Uniform FFTs (NUFFTs) must be used, instead.
Recently, we have proposed a one-dimensional NUFFT using an optimized interpolation window capable to reach an accuracy close to double precision and to gain almost one order of magnitude in terms of root mean square accuracy as compared to state-of-the-art techniques.
In this paper, we extend the approach to the two-dimensional case and apply the 2D NUFFT to radial and spiral MRI scans. The numerical results show the extreme accuracy of the proposed approach.

1 Introduction

In Magnetic Resonance Imaging (MRI), the use of a Cartesian scanning enables image reconstruction with a simple inverse Discrete Fourier Transform (DFT) which can be implemented as a Fast Fourier Transform (FFT) [1]. However, data are often collected under alternative, non-Cartesian acquisitions. For example, spiral scanning [2] is often employed due to its speed thanks to the simpler generation of field gradients. Furthermore, spiral acquisitions fully sample the central part of the k-space which can be used for coil sensitivity estimation and, in general, lead to a more uniform k-space coverage, thus favoring the elimination of artifacts.
The use of standard FFT to process non-Cartesian data breaks down under spiral scans. In this case, MRI imaging requires a more involved processing to guarantee a balance between accuracy and computational burden [3, 4]. Fortunately, Non-Uniform FFT (NUFFT) provide a convenient trade-off in this sense [3–5].
NUFFTs are of different types, depending on whether the destination domain, source domain, or both, are non-uniform. In the first case, the NUFFT is of Non-Equispaced Results (NER), or Type 1; in the second case, it is of Non-Equispaced Data (NED), or Type 2; in the last case, it is of Type 3. NER and NED NUFFTs are of interest in this paper.
Recently, we have presented in [4] an optimized approach for the implementation of NUFFT algorithms, based on a general and new perspective, for all the three types of NUFFTs. The window function involved in the NUFFTs has been optimized to obtain more accurate results than those available in the literature without burdening the computational and memory requirements. However, the approach in [4] has been limited to 1D.
The purpose of this paper is twofold: a) extend [4] to 2D for the NER and NED cases; b) apply the "optimized" 2D NER and NED NUFFTs to a spiral k-space MRI acquisitions under a 2D geometry.
In this paper, the MRI reconstruction problem is tackled by using the Filtered BackProjection (FBP) algorithm [6]. Indeed, FBP is an efficient and effective reconstruction tool that can be applied not only to MRI, but also to other tomographic techniques like x-ray Computed Tomography (CT) [6], nuclear medicine [6] and microwave imaging [7]. Nevertheless, we will consider both, the direct and inverse MRI mapping since both can be of interest when gradient-based, iterative inversion techniques are employed.

2 NUFFT-based MRI Reconstruction

Under a 2D geometry, the signal r acquired by the coils of an MRI system is related to the spin density ρ by the following relation [1]

$$r(k_x(t),k_y(t)) = \iint_O S(x,y)\rho(x,y)e^{-j2\pi[k_x(t)x+k_y(t)y]}dO, \quad (1)$$

where S is the receiving coil sensitivity map, $\underline{k}(t) = (k_x(t),k_y(t))$ denotes the k-space trajectory dictated by the magnetic field gradient, t is the time and O is the Region of Interest (ROI).
Henceforth, we use a pixel-based approximation to discretize ρ and assume to sample the signal r at the time instants t_n. In particular, it is supposed that the pixel centers are arranged on a Cartesian grid (x_h, y_l). Furthermore, for the sake of simplicity, we deal with a unitary receiving coil sensitivity function, namely, $S(x,y) = 1$. Finally, a square ROI $O = [-a,a] \times [-a,a]$ is handled. Accordingly, eq. (1) rewrites as

$$r_n = \sum_{hl} \rho_{hl} e^{-j2\pi[k_x(t_n)h\Delta x + k_y(t_n)l\Delta y]}\Delta x\Delta y, \;\; n = 1,\ldots,N, \quad (2)$$

where $r_n = r(k_x(t_n), k_y(t_n))$, the $\rho_{hl} = \rho(x_h, y_l)$'s are the unknown pixel values, $(\Delta x, \Delta y)$ the pixel size and N is the overall number of samples. Of course, having assumed $a = b$, $\Delta x = \Delta y$.
Henceforth, the x and y components of the k-space trajectory are dealt with as the real and imaginary parts of a complex number k as

$$k(t) = k_x(t) + jk_y(t) = |k(t)|e^{jk(t)}. \tag{3}$$

2.1 FBP for spiral acquisitions

For a continuous case and assuming that the k-space trajectory covers a circular spectral domain A_K, the reconstruction $\rho_R(x,y)$ from Fourier transform data can be expressed as

$$\rho_R(x,y) = \iint_{A_K} r(k_x,k_y) e^{j2\pi[k_x x + k_y y]} dA_K. \tag{4}$$

Considering a coordinate transformation T so that $(k_x,k_y) = T(u,v)$, then the reconstruction formula (4) can be rewritten as

$$\rho_R(x,y) = \iint_{T^{-1}(A_K)} r(k_x(u,v),k_y(u,v)) \; e^{j2\pi[k_x(u,v)x + k_y(u,v)y]} \left| \frac{\partial(k_x,k_y)}{\partial(u,v)} \right| du dv. \tag{5}$$

In the sequel, we use the parameterization $k_x = u\cos(v)$ and $k_y = u\sin(v)$ with K the radius of A_K. Accordingly, eq. (5) becomes [8]

$$\rho_R(x,y) = \int_{-K}^{K} \int_0^{\pi} r(u\cos(v), u\sin(v)) \; e^{j2\pi u[\cos(v)x + \sin(v)y]} |u| du dv, \tag{6}$$

Eq. (6) expresses the FBP formula [9].
In the spiral scanning case, the trajectory is set as

$$k(t) = \lambda \tau^{\alpha}(t) e^{j\omega\tau(t)}, \tag{7}$$

where $\alpha > 1$ determines the amount of oversampling around the origin, λ determines the size of the portion of k-space covered by the spirals and $\omega = 2\pi n_t$, with n_t the number of turns of each spiral in k-space. The dependence of the intermediate parameter τ on t is set according to prescribed physical constraints and to the constraint that $\tau(T_s) = 1$, where T_s is the time required to collect the generic spiral [2]. Using (7), eq. (6) is rewritten using the following change of variables [8]

$$\begin{cases} u = |k(t)| = \lambda \tau^{\alpha}(t) \\ v = k(t) + \theta = \omega\tau(t) + \theta \end{cases} \tag{8}$$

as

$$\rho_R(x,y) = \int_0^{T_s} \int_0^{2\pi} \lambda \tau^{\alpha}(t) \; r\left(\lambda\tau^{\alpha}(t)\cos(\omega\tau(t)+\theta), \lambda\tau^{\alpha}(t)\sin(\omega\tau(t)+\theta)\right) \; e^{j2\pi\lambda\tau^{\alpha}(t)[\cos(\omega\tau(t)+\theta)x + \sin(\omega\tau(t)+\theta)y]} \left|\frac{dk}{dt}\right| \cdot \left|\cos\left(\frac{dk}{dt}, k(t)\right)\right| dt d\theta, \tag{9}$$

where the symbol $\cos(\cdot,\cdot)$ is used to indicate the cosine of the phase difference between $k(t)$ and dk/dt.
According to the above, eq. (9) can be discretized as

$$\rho_R(x_h, y_l) = \sum_n r_n^{(s)} e^{j2\pi[k_{x_n} x_h + k_{y_n} y_l]}, \tag{10}$$

where

$$r_n^{(s)} = \frac{2\pi\Delta t}{P} \lambda \tau^{\alpha}(t_n) \left|\frac{dk}{dt}(t_n)\right| \cdot \left|\cos\left(\frac{dk}{dt}(t_n), k(t_n)\right)\right| \times r\left(k_{x_n}^{(s)}, k_{y_n}^{(s)}\right). \tag{11}$$

3 Using optimized NUFFT in Spiral MRI

We recall that the expression of the 2D Non-Uniform DFT (NUDFT) of NER type of a sequence of "equispaced" samples $\{z_{hl}\}_{h=-H/2 l=-L/2}^{H/2-1 \; L/2-1}$ evaluated at the non-equispaced grid points $\{(\widetilde{k}_{x_n}, \widetilde{k}_{y_n})\}_{n=1}^{N}$ belonging to $\left[-\frac{H}{2}, \frac{H}{2}\right] \times \left[-\frac{L}{2}, \frac{L}{2}\right]$ is [3]

$$\hat{z}_n = \sum_{h=-\frac{H}{2}}^{\frac{H}{2}-1} \sum_{l=-\frac{L}{2}}^{\frac{L}{2}} z_{hl} e^{-j2\pi\widetilde{k}_{x_n}\frac{h}{H}} e^{-j2\pi\widetilde{k}_{y_n}\frac{l}{L}}, \quad n = 1,\ldots,N. \tag{12}$$

Accordingly, eq. (2) can be recast as a 2D NER-NUDFT of the sequence $\{\rho_{hl}\Delta x\Delta y\}_{h=-H/2 l=-L/2}^{H/2-1 \; L/2-1}$ evaluated at the points $\widetilde{k}_{x_n} = k_{x_n} H\Delta x$ and $\widetilde{k}_{y_n} = k_{y_n} L\Delta y$. In other words, non-uniform k-space samples from a Cartesian MRI image can be computed by a 2D NER-NUDFT.
We now recall that the expression of the 2D NUDFT of NED type of a sequence of "not-equispaced" samples $\{z_n\}_{n=1}^{N}$ at the grid points $\{(\widetilde{k}_{x_n}, \widetilde{k}_{y_n})\}_{n=1}^{N}$ is [3]

$$z_{hl} = \sum_{n=1}^{N} \hat{z}_n e^{-j2\pi\widetilde{k}_{x_n}\frac{h}{H}} e^{-j2\pi\widetilde{k}_{y_n}\frac{l}{L}} \tag{13}$$

Table 1. Accuracy of 2D NUFFTs for the spiral scanning.

Problem	RMS KB	RMS opt
Direct	$2.30 \cdot 10^{-10}$	$2.91 \cdot 10^{-11}$
Inverse	$4.20 \cdot 10^{-10}$	$7.09 \cdot 10^{-11}$

with $h = -H/2, \ldots, H/2-1$, $l = -L/2, \ldots, L/2-1$ and where again $\{(\widetilde{k}_{x_n}, \widetilde{k}_{y_n})\}_{n=1}^{N}$ belongs to $\left[-\frac{H}{2}, \frac{H}{2}\right] \times \left[-\frac{L}{2}, \frac{L}{2}\right]$. Therefore, eq. (10) can be recast as a 2D NED-NUDFT of the sequences $\{r_n^{(s)}\}_{n=1}^{N}$ sampled at the points $\widetilde{k}_{x_n} = k_{x_n} H \Delta x$ and $\widetilde{k}_{y_n} = k_{y_n} L \Delta y$.
NUFFT algorithms consist of expressing "non-uniformly" sampled exponentials as a weighted sum of a small number of "uniformly" sampled ones. The weighted summation is obtained by aid of a window function. In [4], an optimized window has been worked out. In this paper, we use the results in [4] to represent, in an optimal way, each non-uniformly sampled exponential appearing in (12) or (13).

4 Numerical Results

The performance of the optimized NUFFT concerning the spiral scanning is here assessed.
In particular, to evaluate the accuracy, a reduced-size test case with a $FOV = 0.2m$ and 64×64 discretized ROI has been considered, with a spiral acquisition having a number of 30 interleaves, $\alpha = 1.5$, $g_m = 0.031T/m$, $s_m = 200T/(m \cdot s)$ and $\lambda = 0.55/\Delta x$.
The developed approach is capable to modulate accuracy and computational complexity. Here, we are testing the NUFFT in the case we are interested to achieving double precision accuracy. Table 1 shows the results of the accuracy analysis when the performance is compared to that of the approach in [3]. Both the direct (NER-NUFFT) and inverse (NED-NUFFT) problems are managed. The reference has been provided by NER- and NED-NUDFTs.
We now show the reconstruction of the Shepp-Logan phantom achieved in the case of a 1024×1024 pixels discretized ROI. Fig. 1 illustrates the obtained reconstruction. As it can be seen, the achieved reconstruction confirms the foreseen accuracy. Finally, Fig. 2 highlights the cuts along the x-axis to better illustrate the comparison between spiral reconstruction and phantom.

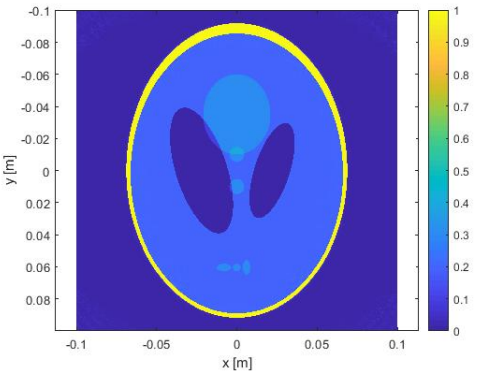

Figure 1. Spiral reconstruction.

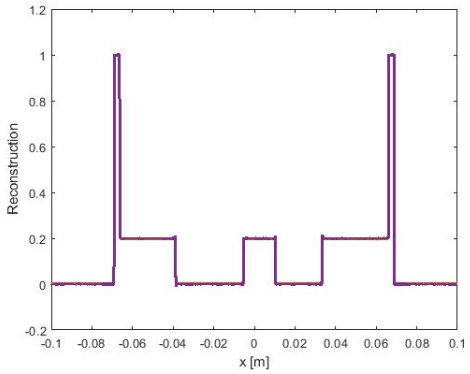

Figure 2. Spiral scanning: x-cut. Red line: reference phantom. Blue line: reconstruction.

References

[1] J.A. Fessler, "Model-based image reconstruction for MRI," *IEEE Signal Proc. Mag.*, vol. 27, n. 4, pp. 81–89, Jul. 2010.

[2] D.-H. Kim, E. Adalsteinsson, D.M. Spielman, "Simple analytic variable density spiral design," *Magn. Res. Med.*, vol. 50, n. 1, pp. 214–219, Jul. 2003.

[3] K. Fourmont, "Non-Equispaced Fast Fourier Transforms with applications to tomography," *J. Fourier Anal. Appl.*, vol. 9, n. 5, pp. 431—450, Sept. 2003.

[4] A. Capozzoli, C. Curcio, A. Liseno, "Optimized Non-Uniform FFTs (NUFFTs) and their application to array factor computation," *IEEE Trans. Antennas Prop.*, vol. 67, n. 6, 3924–3938, Jun. 2019.

[5] A. Capozzoli, C. Curcio, A. Liseno, A. Riccardi, "Parameter selection and accuracy in type-3 non-uniform FFTs based on Gaussian gridding," *Progr. Electromagn. Res.*, vol. 142, 743–770, 2013.

[6] G.L. Zeng, "Model based filtered backprojection algorithm: a tutorial," *Biomed. Eng. Lett.*, vol. 4, pp. 3–18, 2014.

[7] A. Capozzoli, C. Curcio, A. Di Vico, A. Liseno, "NUFFT-& GPU-based fast imaging of vegetation," *IEICE Trans. Commun.*, vol. E94-B, n. 7, pp. 2092–2103, Jul. 2011.

[8] R.D. Hoge, R.K.S. Kwan, G.B. Pike, "Density compensation functions for spiral MRI," *Magn. Res. Med.*, vol. 38, n. 1, pp. 117–128, Jul. 1997.

[9] A.C. Kak, M. Slaney, Principles of Computerized Tomographic Imaging, *IEEE Press*, New York, NY, 1988.